Received: 30 September 2022 | Revised: 20 March 2023 | Accepted: 7 April 2023

https://doi.org/10.1016/j.rpth.2023.100158

rpth research & practice in thrombosis & haemostasis

BRIEF REPORT

Spatial transcriptomics of murine bone marrow megakaryocytes at single-cell resolution

Julia Tilburg PhD[1] | Andrew P. Stone PhD[1] | James M. Billingsley PhD[2] | David K. Scoville PhD[3] | Anna Pavenko AS[3] | Yan Liang PhD[3] | Joseph E. Italiano Jr PhD[1] | Kellie R. Machlus PhD[1]

[1]Department of Surgery, Harvard Medical School and Vascular Biology Program, Boston Children's Hospital, Boston, Massachusetts, USA

[2]Harvard Chan Bioinformatics Core, Department of Biostatistics, Harvard School of Public Health, Boston, Massachusetts, USA

[3]Nanostring Technologies Inc, Seattle, Washington, USA

Correspondence
Kellie R. Machlus, Vascular Biology Program, Boston Children's Hospital, 1 Blackfan Circle, Boston, MA 02115, USA.
Email: Kellie.Machlus@childrens.harvard.edu

Handling Editor: Prof Yotis Senis

Abstract

Background: While megakaryocytes are known for making platelets, recent single-cell RNA sequencing data have revealed subpopulations of megakaryocytes with predicted immunoregulatory and bone marrow niche-supporting roles. Although these studies uncovered interesting information regarding the transcriptional variation of megakaryocytes, the generation, localization, and regulation of these subsets have not yet been studied and therefore remain incompletely understood. Considering the complex organization of the bone marrow, we reasoned that the application of spatial transcriptomic approaches could help dissect megakaryocyte heterogeneity within a spatiotemporal context.

Objectives: The aim of this study was to combine spatial context and transcriptomics to assess the heterogeneity of murine bone marrow megakaryocytes *in situ* at a single-cell level.

Methods: Bone marrow sections were obtained from femurs of C57BL/6J mice. Using the murine whole transcriptome array on the Nanostring GeoMx digital spatial profiling platform, we profiled 44 individual megakaryocytes ($CD41^+$ by immunofluorescence) *in situ* throughout the bone marrow, both adjacent and nonadjacent to the endothelium (directly in contact with vascular endothelial-cadherin–positive cells).

Results: Principal component analysis revealed no association between transcriptomic profile and adjacency to the vasculature. However, there was a significant effect of proximal vs distal regions of the bone. Two and 3 genes were found overexpressed in the proximal and distal sides, respectively. Of note, proplatelet basic protein and platelet factor 4, 2 genes associated with platelet production, had higher expression in proximal megakaryocytes.

Conclusion: This study indicates a possible effect of spatial location on megakaryocyte heterogeneity and substantiate further interest in investigating megakaryocyte subpopulations in the context of their spatial orientation.

Julia Tilburg and Andrew P. Stone contributed equally to this study.

Joseph E. Italiano Jr and Kellie R. Machlus contributed equally to this study.

KEYWORDS
bone marrow, megakaryocytes, spatial transcriptomics, blood platelets, single-cell

Essentials

- Platelet-producing cells in the bone marrow are composed of a varied population.
- New technology can reveal gene expression variation of intact tissues at a single-cell level.
- Gene expression was quantified from single cells with some variation related to cell location.
- Improvements in this technology will help map variation in platelet-producing cells in the marrow.

1 | INTRODUCTION

Megakaryocytes are cells that primarily reside within the bone marrow (BM) and are derived from hematopoietic stem cells via differentiation from progressively restricted progenitors followed by a complex process of maturation including the formation of a demarcation membrane system and polyploidization [1,2]. A pivotal function of megakaryocytes is the generation of platelets through the release of long protrusions called proplatelets into sinusoidal vessels [3,4]. Platelets have important roles in not only hemostasis but also other key biological functions such as angiogenesis and wound healing [5]. Historically, BM megakaryocytes have been considered a phenotypically homogenous population that produces a uniform population of platelets. However, recent studies have challenged this paradigm and created a fundamental shift in how we view both megakaryocytes and their platelet progeny [6,7]. Single-cell RNA sequencing (scRNAseq) of murine BM megakaryocytes revealed transcriptional heterogeneity, which separates megakaryocytes into distinct platelet-producing, immunoregulatory, stem cell niche-supporting, and immature subpopulations [8].

While single-cell technologies are highly informative about transcriptional differences, the spatial context of cells is lost due to the processing and dissociation of tissues that are required for these analyses. As such, the role of megakaryocytes in distinct regions of the bone remains poorly understood. This spatial context with regard to the transcriptional heterogeneity of megakaryocytes is of great interest as localization near, for instance, the vasculature is required for elongation of proplatelets into the vessel lumen [9]. More broadly, it has also been shown that the architecture of the BM can drive distinct hematopoietic functions and specialization in different regions of the bone [10].

Recent technological advancements in spatial transcriptomics have enabled the incorporation of gene expression profiles of tissues *in situ* [11,12]. This allows the integration of morphological, situational, and transcriptional information to classify cells in the context of their microenvironment. Spatial transcriptomic approaches have so far been applied for *in situ* interrogation of different regions of an organ, such as in the brain, or for comparison of tumor and surrounding healthy tissue [13–15]. Here, we present a study of megakaryocytes *in situ* in the femur of mice at a single-cell transcriptomic level, using the Nanostring GeoMx spatial transcriptomics platform.

2 | METHODS

2.1 | Animals

Two C57BL/6J mice, one at 3 and another at 18 months of age, were purchased (Jackson Laboratory). Animals were housed at Boston Children's Hospital before euthanasia using CO_2. All procedures were approved by the institutional animal care and use committee of Boston Children's Hospital.

2.2 | Processing of bones

Femurs were dissected and fixed in 4% paraformaldehyde in phosphate-buffered saline (PBS) for 24 hours at 4 °C. Bones were decalcified for 5 days in 10% EDTA (Sigma) in PBS pH 7.5 with 2 changes of EDTA. Bones were processed using a Thermo Fisher Scientific Excelsior AS with 2× 70% ethanol, 2× 95% ethanol, 3× 100% ethanol, 3× Xylene, and 3× Paraffin, with 1 hour for each step. A Leica tissue embedder was used for embedding. Bones were sectioned at 5-μm thickness on an HM 355s microtome (Thermo Fisher Scientific) and mounted onto Leica Bond Plus microscope slides.

2.3 | Immunofluorescence

Paraffin sections were dewaxed with 2× 5-minute washes in xylene, 2× 5-minute incubations in 100% ethanol, 1× 5 minutes in 95% ethanol, and 1 minute in PBS. For immunofluorescence, slides were baked for 1 hour at 55 °C and antigen retrieval was performed for 20 minutes at high pressure in 10 mM sodium citrate in PBS (pH 6.0) before cooling slides rapidly on ice. Femurs were stained with CD41 and vascular endothelial (VE)–cadherin (all antibodies are listed in Supplementary Table 1) and imaged using an LSM880 confocal microscope (Zeiss LSM 880, with 20× 0.8 NA Zeiss objective), and tile scans of the whole bones were generated.

2.4 | Spatial profiling

For transcriptomic interrogation, slides were baked for 3 hours at 55 °C and rehydrated, followed by heat-induced epitope retrieval (epitope retrieval solution 2 for 20 minutes at 100 °C) and enzymatic digestion (1 μg/mL proteinase K for 15 minutes at 37 °C). The tissue sections were hybridized with the Nanostring mouse whole transcriptome oligonucleotide probe mix overnight and following formamide/saline sodium citrate buffer stringent washes were blocked with donkey serum and incubated with CD41 primary antibody for 1 hour. After washing with saline sodium citrate buffer, secondary antibodies were incubated for 30 minutes. After additional washes, Syto83 and CD31 were also incubated on the slides for 1 hour. Tissue sections were then loaded into the GeoMx platform and regions of interest (ROIs) were selected, guided by the immunofluorescence of the morphology marker antibodies listed above. Of note, a serial section slide was stained with 4',diamidino-2-phenylindole, CD41, and VE-cadherin to confirm the adjacency/nonadjacency allocation of selected megakaryocytes. Following ROI selection, the GeoMx DSP directed UV light at each ROI and released the RNA ID and UMI-containing oligonucleotide tags that were then prepared for sequencing. Illumina i5 and i7 dual-indexing primers were added during polymerase chain reaction (4 μL of collected oligonucleotide/ROI) to uniquely index each ROI. AMPure XP beads (Beckman Coulter) were used for polymerase chain reaction purification. Library concentration was measured using a Qubit fluorimeter (Thermo Fisher Scientific) and quality was assessed using a Bioanalyzer (Agilent). Sequencing was performed on an Illumina NovaSeq 6000 and fastq files were processed by the NanoString DND pipeline, resulting in count data for each target probe in each ROI.

2.5 | Data normalization, analysis, and accessibility

Eighty-three segments (≥70% aligned reads) and 1234 transcript targets (>2 counts over background in ≥5% of segments) were selected for analyses. Raw counts <3 were set to NA. Filtered counts were normalized to the geometric mean of a set of the 5 most stable transcripts identified by GeNorm. For principal component analysis (PCA), NA values were set to the minimum normalized value − 1 and log2 transformed. Differential expression analyses were performed using MAST [16] R package version 1.16.0. All data are available at GEO under the indicated accession number (GSE224838).

2.6 | Distance measurements of megakaryocytes

The distance of individual megakaryocytes from the proximal end of the femurs was calculated using a modified ImageJ macro (https://gist.github.com/lacan/74f550a21ea97f46c74f1a110583586d) that calculated the distance to a user-generated line.

3 | RESULTS AND DISCUSSION

To explore transcriptional heterogeneity in megakaryocytes while retaining spatial information, we investigated murine femurs using the Nanostring GeoMx platform (Figure A). In this platform, megakaryocytes were identified with a CD41-labeling antibody. Forty-four individual megakaryocytes from both 3- and 18-month-old mice were selected using the GeoMx platform by hand drawing an ROI around each cell, guided by CD41 immunofluorescence. Three examples of this selection are shown in Figure B. We then used the mouse whole transcriptome UV-cleavable oligonucleotide probe set that hybridized to the target RNA in the tissue. Next, UV exposure, with an accuracy of 1 μm, was applied specifically within each ROI and sequencing was performed on the released oligonucleotides of each ROI (megakaryocyte) (Figure 1A). From the young sample, 3 ROIs were excluded due to sequencing errors. Megakaryocytes were selected across the length of each femur with positional and morphological characteristics measured (Supplementary Table 2) (proximal, distal, and middle region) and megakaryocytes both directly adjacent and nonadjacent to the vasculature were included. In addition, for the adjacency to the vasculature annotation, we overlaid a serial section to help guide the adjacency/nonadjacency classification by addition of another layer of depth (Figure 1C).

3.1 | Normalization of single-cell spatial transcriptomics data

The resulting single-cell transcriptomic data could not be normalized using conventional normalization strategies for spatial transcriptomic data (ie, normalization to area size or nuclear count), as this would wrongly correct for biologically interesting variables present within megakaryocytes, such as differences in ploidy. To overcome this, we created a method in which a housekeeping gene normalization was performed, for which 5 genes that were ubiquitously expressed across all megakaryocytes were selected (cysteine-rich hydrophobic domain 2 [*Chic2*], *Gm52436*, *Gm52800*, *LOC118568632*, and *LOC11856834*). Suitability for normalization was confirmed using the GeNorm algorithm [17] (Figure 1D). Successful normalization was established by comparison of the geometric mean of the targets before and after normalization, and a correction for extremes was observed (Figure 1E).

3.2 | Clustering analysis of individual megakaryocytes

A total of 19,962 individual genes were detected, and 1234 individual genes exceeded background expression in >5% of megakaryocytes. Of note, this is lower than conventional scRNAseq methodologies where megakaryocytes have been observed to express more genes. [8] We addressed the morphological and positional characteristics associated

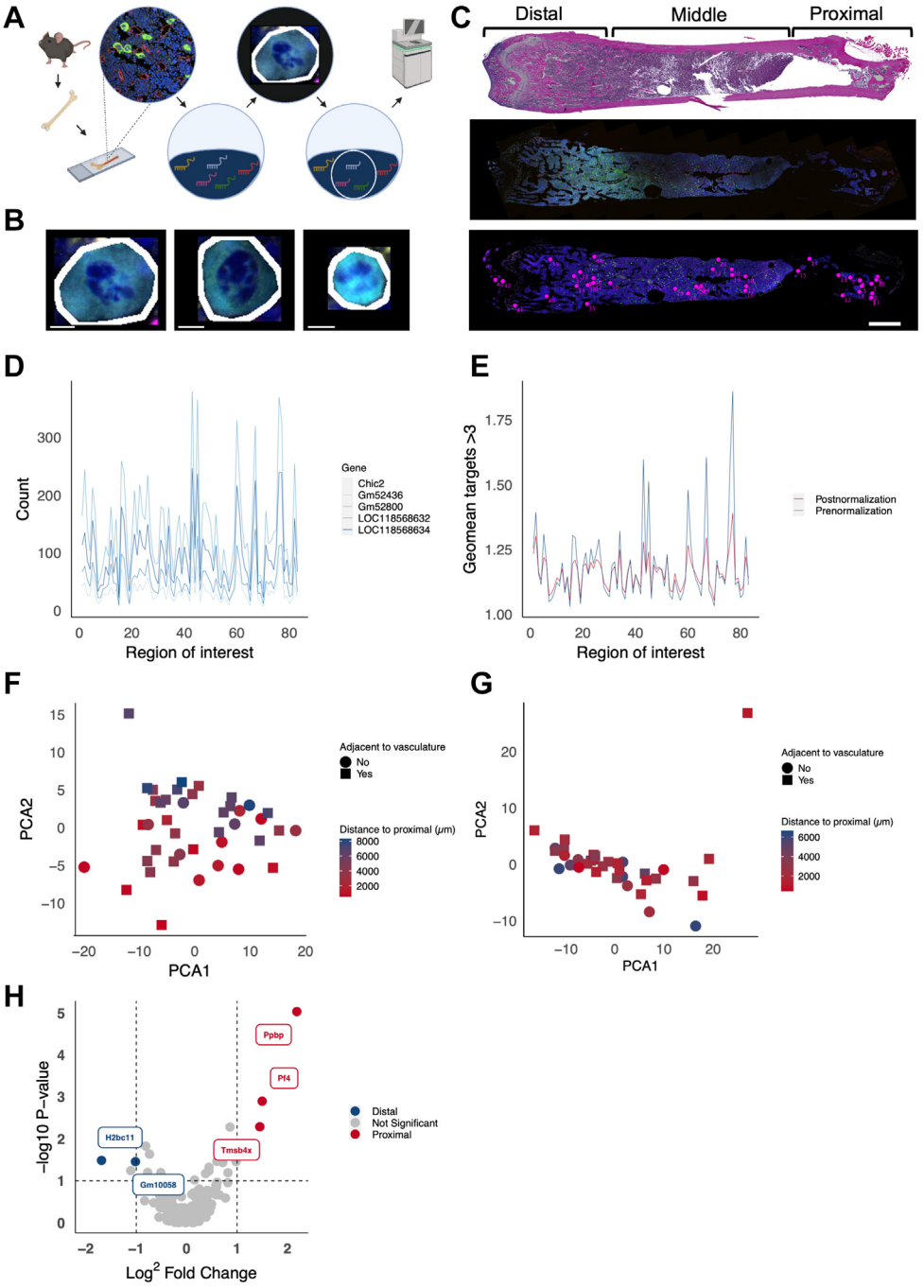

FIGURE 1 GeoMx spatial transcriptomics identifies heterogeneity along the longitudinal axis in a young mouse femur. (A) Schematic of the experimental procedure used for spatial transcriptomics. Dissection of mouse femur, sectioning, immunofluorescent staining for cells of interest, application of mouse whole transcriptome array probeset, region of interest (ROI) selection and UV cleavage, and sequencing of probes within the ROI. (B) Examples of megakaryocytes selected as individual ROIs showing CD41 (cyan) and nuclei (Syto83, blue) expression. The ROI is marked in white. Scale bar is 10 μm (C) Hematoxylin and eosin stain of the tissue section used to guide identification of individual megakaryocytes and their respective localization to the vasculature. Immunofluorescent staining of a serial section was used to help guide ROI selection on the GeoMx Nuclei (blue), VE-cadherin (red), and CD41 (green). Immunofluorescent image of the section used for selection of individual megakaryocytes with the locations of individual megakaryocytes selected for transcriptomic analysis marked (pink dots). Megakaryocytes were selected across the length of each femur (proximal, distal, and middle regions) and megakaryocytes both directly adjacent and nonadjacent to the vasculature were included. Scale bar is 1 mm (D) Absolute counts for 5 probes identified with expression above background in all samples as suitable housekeepers by using the GeNorm algorithm. (E) Gene expression for distinct ROIs before and after normalization shown as the geometric mean of counts for all genes. (F) Principal component analysis (PCA) of gene expression for 1234 genes identified from 41 individual megakaryocytes in the young mouse femur. Color of points is determined by distance from the proximal end of the femur with proximal (red) to distal (blue) distribution. (G) Principal component analysis of gene expression for 1234 genes identified from 36 individual megakaryocytes in the old mouse femur. Color of points is determined by distance from the proximal end of the femur with proximal (red) to the distal (blue) distribution. (H) Volcano plot of differentially expressed genes from megakaryocytes with those genes significantly upregulated ($P < .05$) in the proximal (red) and distal (blue) of the young mouse.

TABLE Top 10 upregulated genes in the proximal and distal regions. Shown are the 10 most differentially upregulated genes in megakaryocytes from a young mouse femur from the proximal and distal regions of the bone marrow, respectively. Shown are the respective fold changes of these genes and their *P* values.

Gene symbol	Gene name	Confidence interval low	Confidence interval high	Fold change	*P*-value
Top 10 proximal					
Ppbp	Proplatelet basic protein	1.236	3.135	4.548	.000009
Pf4	Platelet factor 4	0.538	2.455	2.821	.001
Tmsb4x	Thymosin, beta 4, X chromosome	0.454	2.445	2.731	.005
Itga2b	Intergrin subunit alpha 2b	0.019	1.698	1.813	.005
Ptms	Parathymosin	−0.172	1.367	1.513	.03
Gm40469	Gm40469	0.057	1.901	1.971	.04
Cd9	Cd9	−0.146	1.576	1.642	.04
Lrr1	Leucine-rich repeat protein 1	−0.140	1.023	1.358	.05
Ccdc71l	Coiled-coil domain containing 71 like	−0.278	1.160	1.358	.06
Zfp808	Zink finger protein 808	−0.173	1.809	1.763	.06
Top 10 distal					
Rps11	Ribosomal protein S11	−1.610	−0.020	0.568	.01
Phgdh	Phosphoglycerate dehydrogenase	−1.458	−0.020	0.599	.02
H2bc11	H2B clustered histone 11	−2.597	−0.786	0.310	.03
Gm10058	Gm10058	−1.959	−0.075	0.494	.04
Potefam3e	POTE ankyrin domain family member 3E	−2.129	−0.092	0.463	.06
Cyp2d12	Cytochrome P450, family 2, subfamily 2, subfamily d, polypeptide 12	−1.823	0.271	0.584	.06
Rps23rg1	Ribosomal protein S23 retrogene 1	−1.115	0.085	0.700	.06
Rpl21	Ribosomal protein L21	−1.421	0.360	0.692	.09
Rps18	Ribosomal protein S18	−1.082	0.310	0.765	.13
Rps2	Ribosomal protein S2	−1.891	0.211	0.559	.14

with unique megakaryocytes by PCA. In the young sample, adjacency to vasculature was not found to correlate with transcriptome variation (Figure 1F, $P = .17$). This is noteworthy, as previous work that examined sections stained for a protein, which megakaryocyte scRNAseq data identified as upregulated in the proplatelet subpopulation, found that megakaryocytes positive for this protein are in closer proximity to the vasculature [8]. However, PCA did reveal a significant correlation between gene expression and the distance of the megakaryocytes assayed from the proximal end of the bone ($P = .0002$). In the femur from the aged mouse, no effect of morphological characteristics or clustering was observed (Figure 1G).

3.3 | Differential expression proximity on the length of the bone

When analyzing transcriptional heterogeneity based on the distance of megakaryocytes to the proximal side of the femur, 3 genes were upregulated in the proximal and 2 in the distal regions of the bone (fold change > 1, $P < .05$) (Figure 1H, top 10 differentially expressed genes are reported in the Table). Of note, among the genes upregulated in proximal region megakaryocytes of this sample were platelet factor 4 (*Pf4*) and proplatelet basic protein (*Ppbp*); these are both alpha granule proteins and thereby packaged into platelets [18,19]. Whether this could be indicative of a higher abundance of platelet-producing megakaryocytes within the proximal region of the BM could be an avenue for future investigation.

3.4 | Limitations and future perspective

Spatial transcriptomics is an exciting new approach that applies the very latest in sequencing technologies to study transcriptional heterogeneity while retaining morphological data from native tissue. Several limitations arose while applying this novel technology to single megakaryocytes for the first time. First, the sequencing depth was limited, and although genes known for expression in megakaryocytes were detected, a higher depth will be beneficial to include less highly expressed genes and fully leverage the whole transcriptome aspect of the technology. Second, because the GeoMx platform requires

collection of sequencing oligonucleotides after extraction from the tissue, the number of ROIs, and, therefore, the number of individual megakaryocytes that can be included is limited. Lastly, one of the key features of megakaryocyte maturation is nuclear ploidy, and transcriptomic heterogeneity has been previously linked to this characteristic [8]. Unfortunately, the use of 5-μm sections does not allow for the accurate determination of ploidy.

Although single-cell spatial transcriptomics has come very far in a short period of time, there remains a triad of compromise; the current platforms only optimize 2 of the 3 most important parameters selecting between the ROI number, transcript number, and depth of quantification [20]. For example, while the GeoMx is highly capable at performing a thorough quantification of larger areas, it has limitations in the quantification of single cells as we demonstrated [21]. There are emerging methods, such as those based upon massively multiplexed fluorescence-in-situ-hybridization technologies that are solely focused on smaller ROIs; however, the multiplexing of these platforms is currently limited versus sequencing-based technologies [15]. Even though 1234 genes is a smaller data set compared to those of traditional scRNAseq technologies, to our knowledge, this is the highest-plex spatially resolved single megakaryocyte data set to date [8]. With spatial transcriptomics technology rapidly evolving and advancing, we predict that more in-depth interrogation of the spatial transcriptomics of megakaryocytes will be feasible at a larger scale within the near future.

3.5 | Conclusion

In sum, we present a technical report summarizing our application of a single-cell spatial whole transcriptome approach to quantify RNAs of individual BM megakaryocytes in a mouse femur *in situ*. An effect of megakaryocyte transcriptome on proximity along the axis of the femur was detected in a young mouse, with *Pf4* and *Ppbp* showing significantly enhanced expression in the proximal side of the bone. In the future, further validation experiments and investigation of this heterogeneity will elucidate the biological implication of these observations. However, these studies substantiate further interest in investigating megakaryocyte heterogeneity in the complexity of their spatial orientation. Technological advancements in multiplexing, resolution, and single-cell throughput of spatial transcriptomics will hopefully facilitate the development of a megakaryocyte BM transcriptomic atlas and will overcome the limitations of current technologies. Such an atlas will increase our understanding in the generation, localization, and regulation of subpopulations of megakaryocytes.

ACKNOWLEDGMENTS

The authors thank Li Zhang from the Harvard Rodent histopathology core for embedding the tissues. The authors thank Abdullah Khan for commenting on the manuscript. Figure A is produced using BioRender.

FUNDING

J.T. is supported by a Rubicon grant from The Netherlands Organization for Health Research and Development (452020206). J.I. is supported by the National Institute of Health National Heart, Lung and Blood Institute (R01HL68130, R35HL161175). K.R.M. is supported by grants from the National Institutes of Health, National Institute of Diabetes and Digestive and Kidney Diseases (R03DK124746) and National Heart, Lung, and Blood Institute (R01HL151494) and is an American Society of Hematology Scholar.

ETHICS STATEMENT

All procedures were approved by the institutional animal care and use committee of the Boston Children's Hospital.

AUTHOR CONTRIBUTIONS

J.T. and A.S. designed the study, performed experiments, performed analysis, and wrote the manuscript; J.B. performed analysis; D.S., A.P., and Y.L. performed experiments; and J.I. and K.R.M. designed the study and revised the manuscript. All authors commented on the manuscript.

RELATIONSHIP DISCLOSURE

J.T., A.S., and K.R.M. report no conflicts of interest; J.I. has financial interest in and is a founder of PlateletBio, a biotechnology company focused on making donor-independent platelet-like cells at scale. The interests of J.I. are managed by Boston Children's Hospital.

TWITTER

Julia Tilburg @julia_tilburg
Andrew P. Stone @andystone93
Joseph E. Italiano Jr. @JosepItaliano
Kellie R. Machlus @theclotthickens

REFERENCES

[1] Tilburg J, Becker IC, Italiano JE. Don't you forget about me(gakaryocytes). *Blood*. 2022;139:3245–54.
[2] Noetzli LJ, French SL, Machlus KR. New insights into the differentiation of megakaryocytes from hematopoietic progenitors. *Arterioscler Thromb Vasc Biol*. 2019;39:1288–300.
[3] Bender M, Thon JN, Ehrlicher AJ, Wu S, Mazutis L, Deschmann E, et al. Microtubule sliding drives proplatelet elongation and is dependent on cytoplasmic dynein. *Blood*. 2015;125:860–8.
[4] Italiano JE, Lecine P, Shivdasani RA, Hartwig JH. Blood platelets are assembled principally at the ends of proplatelet processes produced by differentiated megakaryocytes. *J Cell Biol*. 1999;147:1299–312.
[5] Italiano Jr JE, Richardson JL, Patel-Hett S, Battinelli E, Zaslavsky A, Short S, et al. Angiogenesis is regulated by a novel mechanism: pro- and antiangiogenic proteins are organized into separate platelet alpha granules and differentially released. *Blood*. 2008;111:1227–33.
[6] Wang H, He J, Xu C, Chen X, Yang H, Shi S, et al. Decoding human megakaryocyte development. *Cell Stem Cell*. 2021;28:535–49.e8.
[7] Liu C, Wu D, Xia M, Li M, Sun Z, Shen B, et al. Characterization of cellular heterogeneity and an immune subpopulation of human megakaryocytes. *Adv Sci (Weinh)*. 2021;15:e2100921.

[8] Sun S, Jin C, Si J, Lei Y, Chen K, Cui Y, et al. Single-cell analysis of ploidy and the transcriptome reveals functional and spatial divergency in murine megakaryopoiesis. *Blood*. 2021;138:1211–24.

[9] Stegner D, vanEeuwijk JMM, Angay O, Gorelashvili MG, Semeniak D, Pinnecker J, et al. Thrombopoiesis is spatially regulated by the bone marrow vasculature. *Nat Commun*. 2017;8:127.

[10] Zhang J, Wu Q, Johnson CB, Pham G, Kinder JM, Olsson A, et al. In situ mapping identifies distinct vascular niches for myelopoiesis. *Nature*. 2021;590:457–62.

[11] Moses L, Pachter L. Museum of spatial transcriptomics. *Nat Methods*. 2022;19:534–46.

[12] Marx V. Method of the year: spatially resolved transcriptomics. *Nat Methods*. 2021;18:9–14.

[13] Berglund E, Maaskola J, Schultz N, Friedrich S, Marklund M, Bergenstråhle J, et al. Spatial maps of prostate cancer transcriptomes reveal an unexplored landscape of heterogeneity. *Nat Commun*. 2018;9:2419.

[14] Hunter MV, Moncada R, Weiss JM, Yanai I, White RM. Spatially resolved transcriptomics reveals the architecture of the tumor-microenvironment interface. *Nat Commun*. 2021;12:6278.

[15] Zhang M, Eichhorn SW, Zingg B, Yao Z, Cotter K, Zeng H, et al. Spatially resolved cell atlas of the mouse primary motor cortex by MERFISH. *Nature*. 2021;598:137–43.

[16] Finak G, McDavid A, Yajima M, Deng J, Gersuk V, Shalek AK, et al. MAST: a flexible statistical framework for assessing transcriptional changes and characterizing heterogeneity in single-cell RNA sequencing data. *Genome Biol*. 2015;16:278.

[17] Vandesompele J, De Preter K, Pattyn F, Poppe B, Van Roy N, De Paepe A, et al. Accurate normalization of real-time quantitative RT-PCR data by geometric averaging of multiple internal control genes. *Genome Biol*. 2002;3:RESEARCH0034.

[18] Lador A, Leshem-Lev D, Spectre G, Abelow A, Kornowski R, Lev EI. Characterization of surface antigens of reticulated immature platelets. *J Thromb Thrombolysis*. 2017;44:291–7.

[19] Blair P, Flaumenhaft R. Platelet alpha-granules: basic biology and clinical correlates. *Blood Rev*. 2009;23:177–89.

[20] Moffitt JR, Lundberg E, Heyn H. The emerging landscape of spatial profiling technologies. *Nat Rev Genet*. 2022;23:741–59.

[21] Jour G, Illa-Bochaca I, Ibrahim M, Donnelly D, Zhu K, Miera EV, et al. Genomic and transcriptomic analyses of NF1-mutant melanoma identify potential targeted approach for treatment. *J Invest Dermatol*. 2023;143:444–55.

SUPPLEMENTARY MATERIAL

The online version contains supplementary material available at https://doi.org/10.1016/j.rpth.2023.100158